Electronic Supplementary Information (ESI) for

MnOOH/Nitrogen-Doped Graphene Hybrid Nanowires Sandwiched by Annealing Graphene Oxide Sheets for Flexible All-Solid-State Supercapacitors

Shuhua Yang, Xuefeng Song, Peng Zhang, Lian Gao**

State Key Laboratory for Metallic Matrix Composite Materials,

School of Materials Science and Engineering,

Shanghai Jiao Tong University, Shanghai, 200240, China.

E-mail address: liangao@mail.sic.ac.cn (L. Gao); songxfeng@sjtu.edu.cn (X. Song)

Tel: +86-12-52412718. Fax: +86-21-52413122

Part I: Calculations

Areal capacitance for the flexible freestanding MNGHNs/AGO sandwich film, and volumetric capacitance, energy density, and power density for the MNGHNs/AGO flexible all-solid-state SCs.

Areal capacitance values of the flexible freestanding MNGHNs/AGO sandwich film were obtained by $C_a=I\Delta t/\Delta ES$, where Δt is the discharge time (seconds), I is the discharge current (A), ΔE is the operating potential window (V) during the discharge, and S is the working area of the electrodes (cm^2).[1]

The volumetric capacitances for the MNGHNs/AGO flexible all-solid-state SCs were calculated from the discharge curves by the following equations:[2]

$$C_v=I\Delta t/V\Delta U \quad (1)$$

where C_v is the volumetric capacitance, I is the discharge current, Δt is the discharge time, ΔU is the potential window during the discharge process, and V (cm^3) was the volume of the whole SCs device (including electrodes, separator and electrolyte).

The volumetric energy (E) and power density (P) of the whole all-solid-state SCs were calculated from the discharge curves using the following equations:[3]

$$E=0.5C_v(\Delta U)^2/3600 \quad (2)$$

$$P=E/\Delta t \quad (3)$$

where E (mWh cm^{-3}) is the energy density, Cv is the volumetric capacitance, ΔU was the SCs voltage window, P (W cm^{-3}) is the power density, and Δt is the discharge time.

References

[1] X. Xiao, X. Peng, H. Jin, T. Li, C. Zhang, B. Gao, B. Hu, K. Huo, J. Zhou, *Adv. Mater.* 2013, 25, 5091.

[2] X. Lu, M. H. Yu, T. Zhai, G. Wang, S. Xie, T. Lu, C. Liang, Y. X. Tong, Y. Li, *Nano Lett.* 2013, 13, 2628.

[3] R. Rakhi, W. Chen, D. Cha, H. Alshareef, *Nano Lett.* 2012, 12, 2559.

Part II: Charge Storage Mechanism

The principal charge storage mechanism involved in the charging and discharging process for MNGHNs/AGO all-solid-state supercapacitors could be assigned to a variation of the manganese valency from III to IV. Redox reactions occurring in the supercapacitor devices involve proton insertion between the positive and negative electrodes which can be represented as follows:[1, 2]

Positive electrode

Discharge: $MnOOH \rightarrow MnO_2H_{1-\delta} + \delta H+ + \delta e$ (6)

Charge: $MnO_2H_{1-\delta} + \delta H+ + \delta e \rightarrow MnOOH$ (7)

Negative electrode

Discharge: $MnO_2 + \delta H+ + \delta e \rightarrow MnO_2H_\delta$ (8)

Charge: $MnO_2H_\delta \rightarrow MnO_2 + \delta H+ + \delta e$ (9)

For MnOOH, it has an inherent redox capability for facile electron-transfer processes and is the main electroactive species for the charge storage/delivery in the redox transition of the corresponding oxide. [3, 4] Besides MnOOH, analogous results for NiOOH and CoOOH have been also reported by G. W. Yang and Y. X. Tong.[5, 6]

References

[1] S. C. Pang, M. A. Anderson, T. W. Chapman, *J. Electrochem. Soc.* 2000, 147, 444.
[2] M. Toupin, T. Brousse, D. Bélanger, *Chem. Mater.* 2004, 16, 3184.
[3] H. T. Tan, X. Rui, W. Shi, C. Xu, H. Yu, H. E. Hoster, Q. Yan, *ChemPlusChem* 2013, 78, 554.
[4] L. Wang, D. L. Wang, *Electrochim. Acta* 2011, 56, 5010.
[5] H. Li, M. Yu, F. Wang, P. Liu, Y. Liang, J. Xiao, C. Wang, Y. Tong, G. Yang, *Nat. Commun.* 2013, 4, 1894.
[6] H. Li, M. Yu, X. Lu, P. Liu, Y. Liang, J. Xiao, Y. Tong, G. Yang, *ACS Appl. Mater. Interfaces* 2014, 6, 745.

Part III: Supplementary Figures

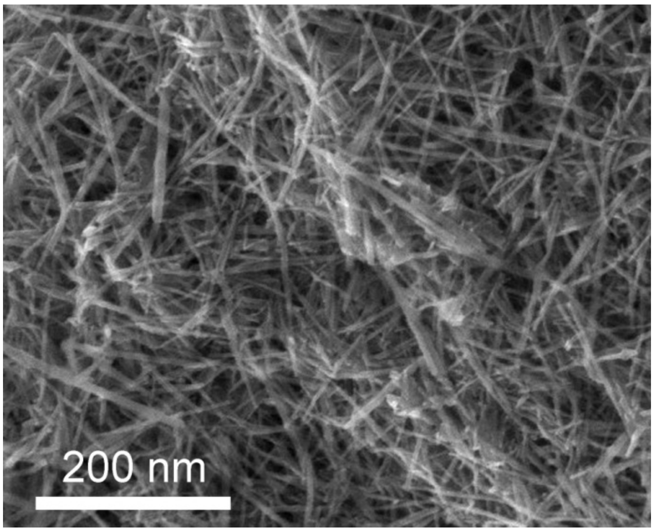

Fig. S1. SEM image of MNGHNs

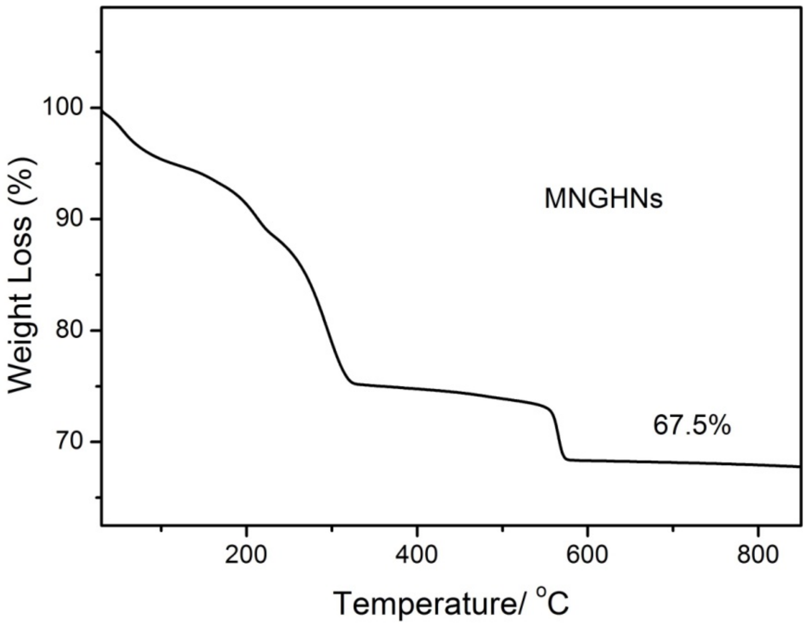

Fig. S2. TGA curve of MNGHNs.

The experiments were performed from 30 to 850 °C in air flow at a heating rate of 10 °C/min. In the process, the NG sheets were burned up, whereas MnOOH turned into Mn_2O_3. Accordingly, the mass ratio of MnOOH is 75.2 wt % in the MNGHNs.

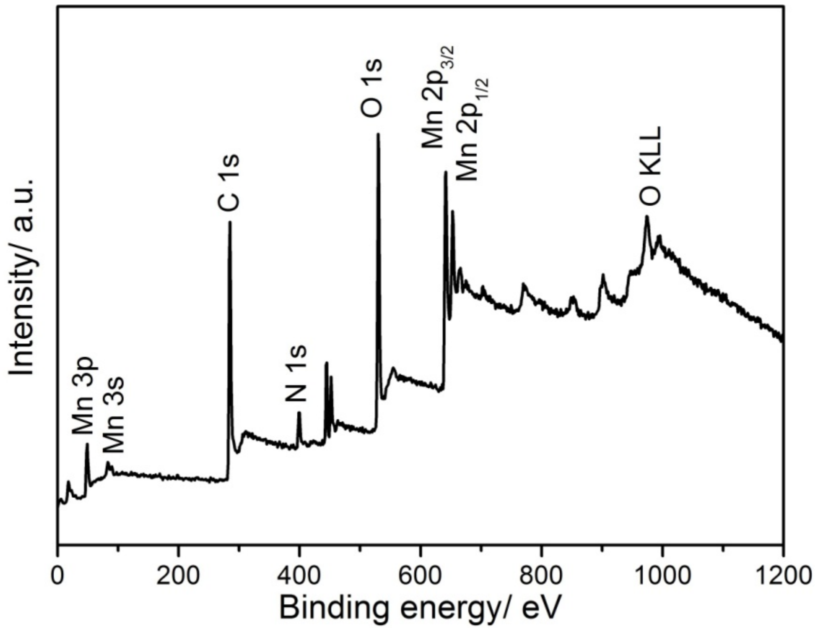

Fig. S3. XPS survey spectra of MNGHNs.

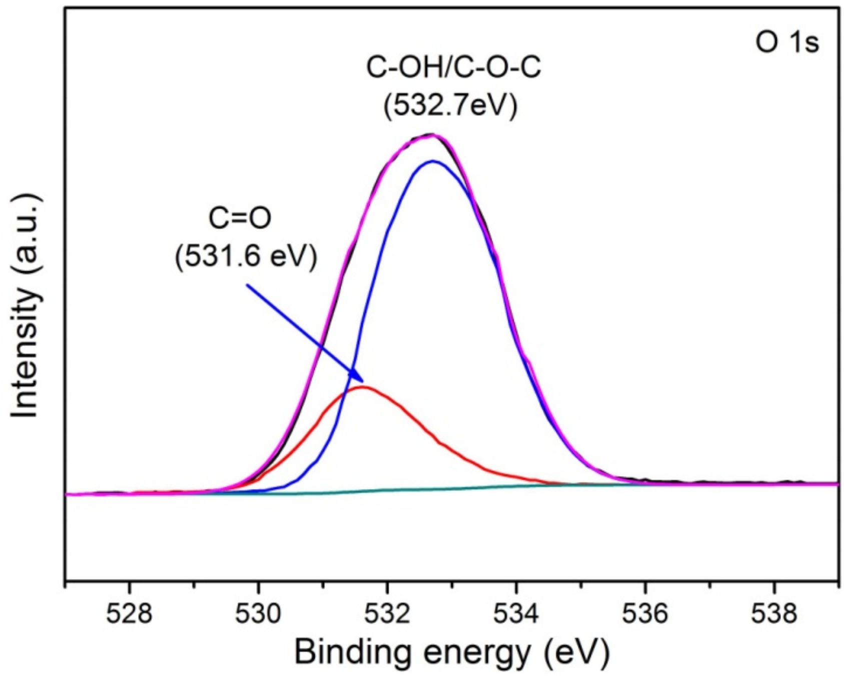

Fig. S4. Narrow O 1s XPS spectra of the graphene.

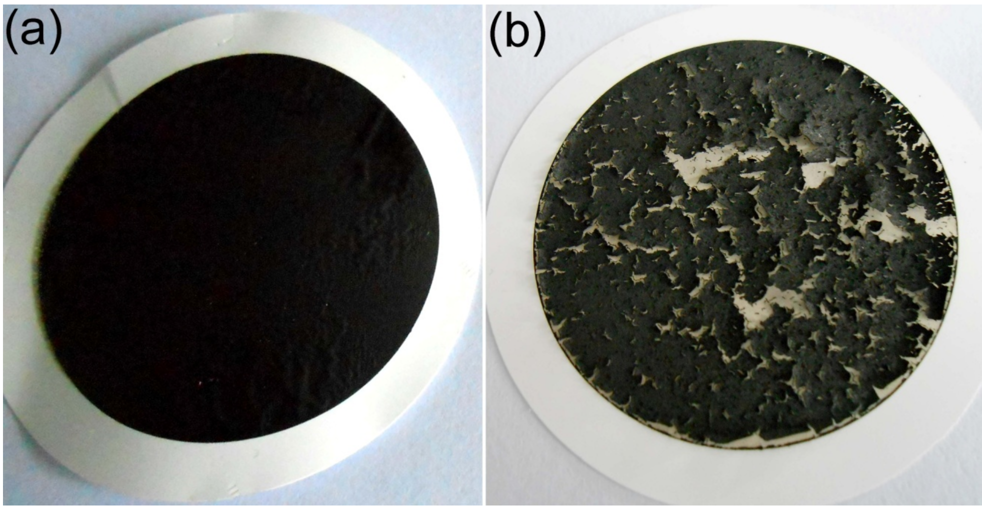

Fig. S5. Digital images of (a) freestanding MNGHNs/AGO sandwich film, and (b) freestanding MNGHNs/RGO sandwich film. The MNGHNs in MNGHNs/AGO sandwich film (or MNGHNs/RGO sandwich film) was about 80% of the whole weight.

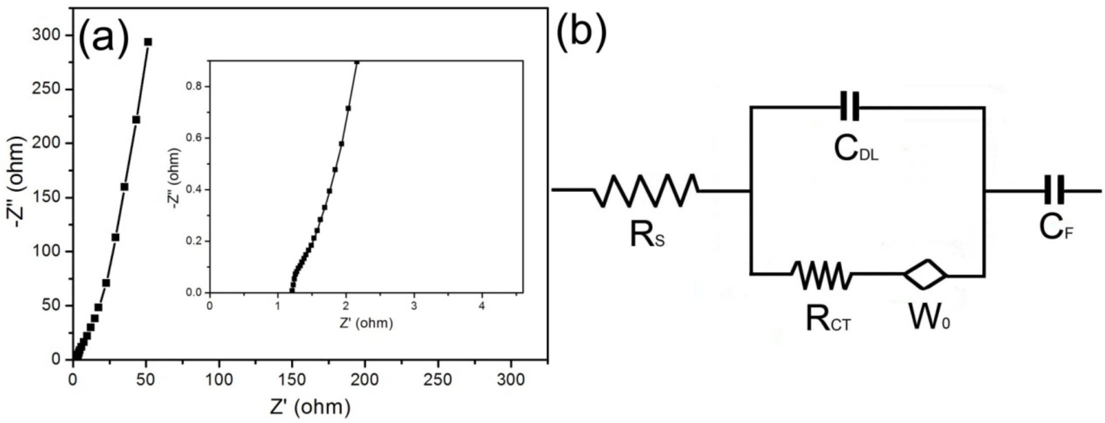

Fig. S6. (a) EIS of the flexible freestanding MNGHNs/AGO sandwich film. The inset shows the enlarged EIS at the high frequency region. (b) The electrical equivalent circuit used for fitting impedance spectra.

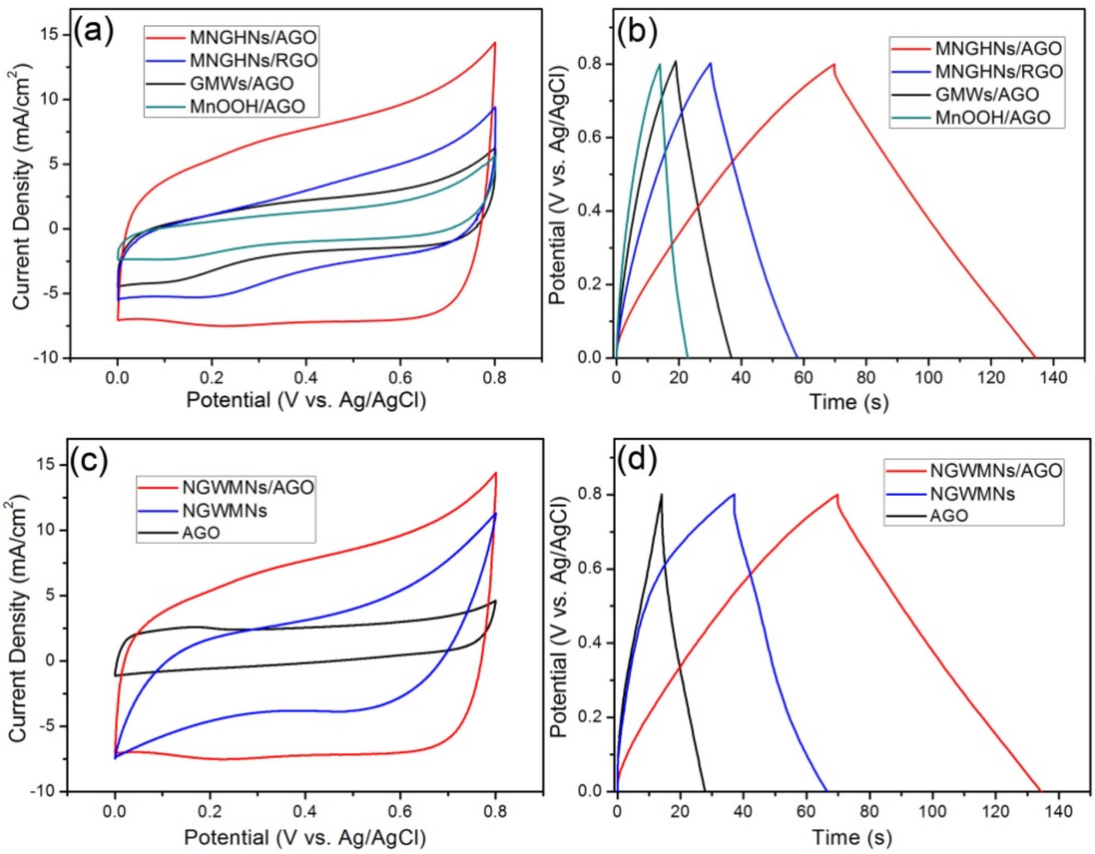

Fig. S7. (a, c) CV curves at a scan rate of 50 mV/s, and (b, d) CD curves at 2 mA/cm^2 in 1 M Na_2SO_4 aqueous electrolyte for MNGHNs/AGO, MNGHNs/RGO, GMWs/AGO, and MnOOH/AGO sandwich films (and pure AGO and MNGHNs electrode made by mixing the samples, acetylene black, and a polyvinylidene dilfluoride (PVDF) binder in a mass ratio of 70 : 20 : 10 in N-methyl pyrrolidone (NMP) solvent, and then pressing the mixture onto the nickel foam substrate (1 cm×1 cm)), respectively.

The electrochemical properties of the MNGHNs/RGO, GMWs/AGO, and MnOOH/AGO sandwich films obtained by replacing AGO with RGO or replacing MNGHNs with GMWs (or MnOOH) for comparison with the as-prepared MNGHNs/AGO sandwich film.

For comparison, all films contain the same mass loading (2 mg/cm^2) and active area (1×1.65 cm^2). All the electrochemical performances of each electrode were measured under the same experimental conditions (three electrode cells, 1 M Na_2SO_4 aqueous solution as electrolyte).

Cyclic voltammetry (CV) measurements were performed at a scan rate of 50 mV/s, as shown in Fig. S6a. The relatively rectangular and symmetric CV curves of four sandwich films indicate the ideal capacitive nature of the fabricated electrodes. However, the MNGHNs/AGO sandwich film exhibits the highest specific capacity, basing on the integral area of CV. Moreover, galvanostatic charge-discharge (CD) measurements were carried out at a current density of 2 mA/cm^2. According to Fig. S6b, the specific capacitances of the four different electrodes are calculated to be 161.5, 70.3, 45.5, and 22.3 mF/cm^2, respectively. Obviously, the MNGHNs/AGO sandwich film shows the highest capacity among the four samples at the same current density, which is consistent with the CV results (Fig. S6a). In addition, the electrochemical properties of the

MNGHNs/AGO sandwich film also compared with those of pure AGO and MNGHNs electrode. The capacitive performance of pure AGO and MNGHNs electrode significantly smaller than that of MNGHNs/AGO sandwich film. The significantly improved capacitance of the MNGHNs/AGO sandwich film can be attributed to synergetic effect of the MNGHNs and AGO.

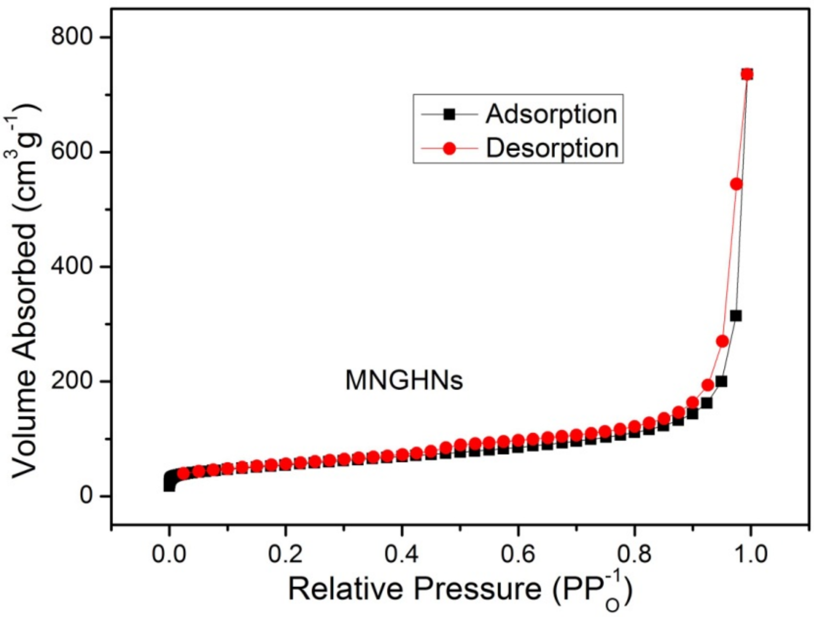

Fig. S8. Nitrogen adsorption and desorption isotherms of MNGHNs.

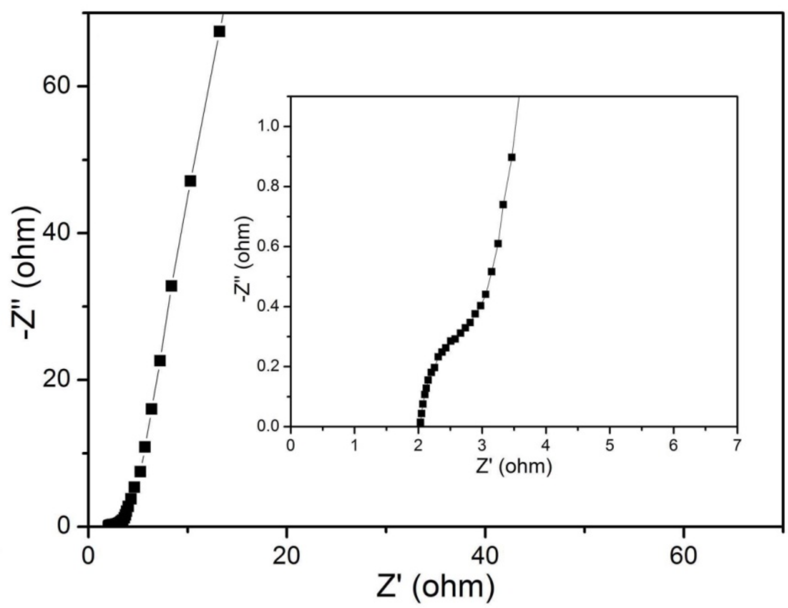

Fig. S9. EIS of MNGHNs/AGO all-solid-state SC under a curvature of 90º. The inset shows the enlarged EIS at the high frequency region.

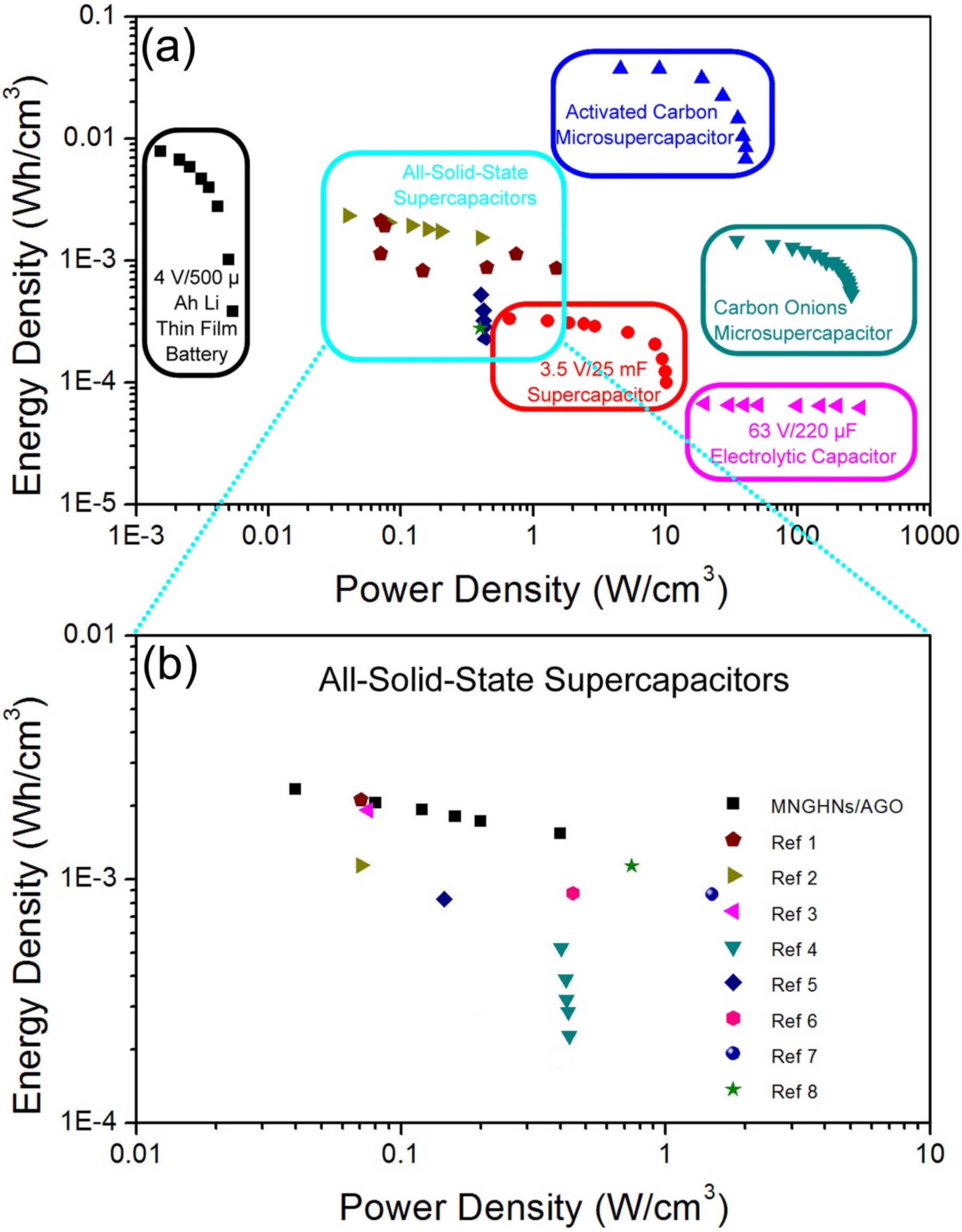

Fig. S10. (a) The Ragone plot for MNGHNs/AGO all-solid-state SC device, compared with the results of typical literature reported previously.[1-9] The plot was made based on the Fig. 4 in the study reported by Prof. P. Simon and co-workers.[9] Compared with the other energy storage devices, the MNGHNs/AGO flexible all-solid-state SC exhibits excellent energy-power characteristics. (b) The magnified plot for various all-solid-state SCs in (a).

The Ragone plots include a 500-μAh thin-film lithium battery, a 25-mF supercapacitor, and a 220-μF electrolytic capacitor, which are made based on the Fig. 4 in the study reported by Prof. P. Simon and co-workers (Fig. S9a),[9] along with other all-solid-state SCs reported previously (Fig. S9b)[1-8] for comparison with our results. The plots show the volumetric energy density and power density of various devices. The MNGHNs/AGO all-solid-state SC exhibits energy densities of up to 2.34 mWh/cm^3. Additionally, the results are superior to most of the results reported by other groups for all-solid-state SC (Fig. S9b). It should be noted that Fig. S9 is used only to show the general range of our devices because different current densities and various calculations were used in the cited data.

References

[1] M. F. El-Kady, V. Strong, S. Dubin, R. B. Kaner, *Science* **2012**, 335, 1326.

[2] M. Kaempgen, C. K. Chan, J. Ma, Y. Cui, G. Gruner, *Nano Lett.* **2009**, 9, 1872.

[3] Y. Xu, Z. Lin, X. Huang, Y. Liu, Y. Huang, X. Duan, *ACS Nano* **2013**, 7, 4042.

[4] X. Xiao, X. Peng, H. Jin, T. Li, C. Zhang, B. Gao, B. Hu, K. Huo, J. Zhou, *Adv. Mater.* **2013**, 25, 5091.

[5] Y. J. Kang, H. Chung, C. H. Han, W. Kim, *Nanotechnology* **2012**, 23, 065401.

[6] Z. Weng, Y. Su, D. W. Wang, F. Li, J. Du, H. M. Cheng, *Adv. Energy Mater.* **2011**, 1, 917.

[7] B. G. Choi, S. J. Chang, H. W. Kang, C. P. Park, H. J. Kim, W. H. Hong, S. Lee, Y. S. Huh, *Nanoscale* **2012**, 4, 4983.

[8] B. G. Choi, J. Hong, W. H. Hong, P. T. Hammond, H. Park, *ACS Nano* **2011**, 5, 7205.

[9] D. Pech, M. Brunet, H. Durou, P. Huang, V. Mochalin, Y. Gogotsi, P. L. Taberna, P. Simon, *Nat. Nanotechnol.* **2010**, 5, 651.

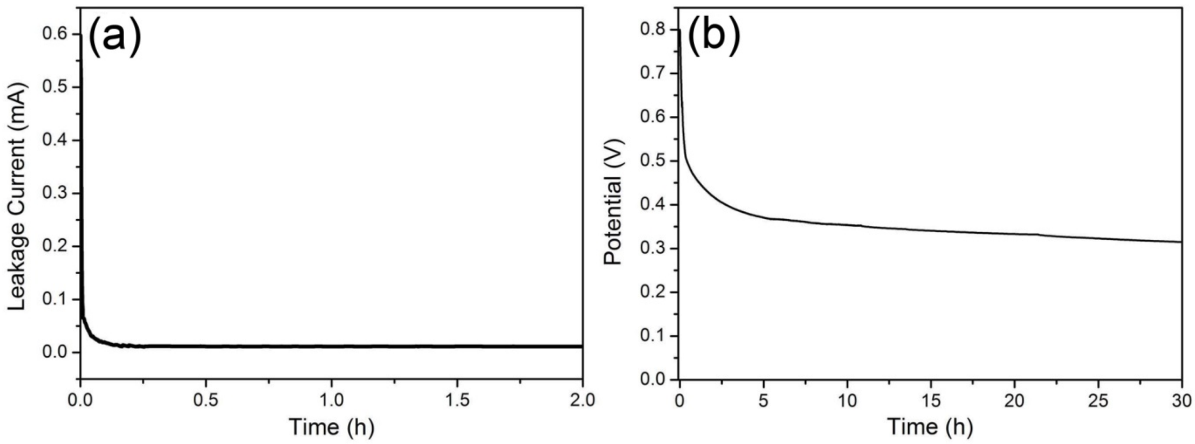

Fig. S11. (a) Leakage current and (b) Self-discharge curves for MNGHNs/AGO all-solid-state SC.

For the leakage current test, the device was first charged to 0.8 V at 2 mA and then the potential was kept at 0.8 V for 2 h while acquiring the current data. For the self-discharge test, the device was first charged to 0.8 V at 2 mA and kept at 0.8 V for 15 min, and then the open potential of the device was recorded as a function of time.

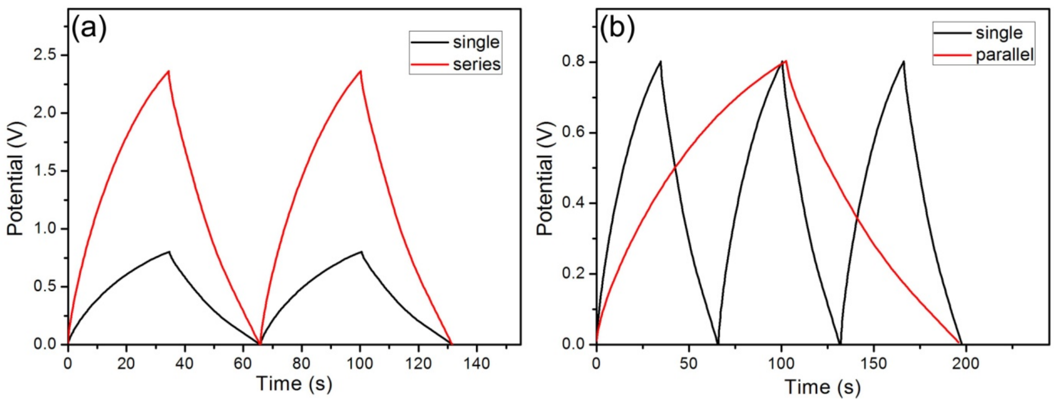

Fig. S12. CD curves at 0.5 A/cm^3 of (a) a single all-solid-state SC (black) and three all-solid-state SCs in series (red), and (b) a single all-solid-state SC (black) and three all-solid-state SCs in parallel (red).

Table S1. Thickness and mass loading ever reported for free standing films for comparison with our results.

Materials	Thickness (μm)	Mass loading (mg/cm^2)	Ref.
MoS_2/Graphene	10-20	4	1
graphene/MnO_2/CNTs	30	2.02	2
VN/CNT	48	4	3
CuO/Graphene	~10	N/A	4
Graphene/MnO_2	~10	N/A	5
Activated carbon	50±5	3.2	6
Graphene Hydrogel	120	~2	7
3D graphene/MnO_2	200-300	0.4	8
CNT/Si	4	0.5	9
V_2O_5/MWNCT	N/A	3-5	10
$Ni(OH)_2$ /3D Graphite	37±3	0.2	11
Graphene-TiO_2	2.6-9.3	1.03-1.26	12
Fe_3O_4/graphene	12.3	~1.7	13
SnO_2/SP-Li	5	0.5	14
MNGHNs/AGO	~16	2	This work

According to Table 1, the MNGHNs/AGO sandwich film achieves a high mass loading of 2 mg/cm^2 with a film thickness of ~16 μm, which is much higher than that of carbon nanotube-based films and three-dimensional (3 D) architecture films, and comparable to two-dimensional (2 D) architecture films, such as MoS_2/Graphene film with a mass loading of 4 mg/cm^2 and a film thickness of 10-20 μm, indicating that the as-fabricated film electrodes offer high mass loading.

References

[1] L. David, R. Bhandavat and G. Singh, *ACS Nano*, 2014, **8**, 1759.
[2] Y. Cheng, S. Lu, H. Zhang, C. V. Varanasi and J. Liu, *Nano Lett.*, 2012, **12**, 4206.
[3] X. Xiao, X. Peng, H. Jin, T. Li, C. Zhang, B. Gao, B. Hu, K. Huo and J. Zhou, *Adv. Mater.*, 2013, **25**, 5091.
[4] Y. Liu, W. Wang, L. Gu, Y. Wang, Y. Ying, Y. Mao, L. Sun and X. Peng, *ACS Appl. Mater. Interfaces*, 2013, **5**, 9850.
[5] A. Yu, H. W. Park, A. Davies, D. C. Higgins, Z. Chen and X. Xiao, *The Journal of Physical Chemistry Letters*, 2011, **2**, 1855.
[6] R. Hastak, P. Sivaraman, D. Potphode, K. Shashidhara and A. Samui, *Electrochim. Acta*, 2012, **59**, 296.
[7] Y. Xu, Z. Lin, X. Huang, Y. Liu, Y. Huang and X. Duan, *ACS Nano*, 2013, **7**, 4042.
[8] Y. He, W. Chen, X. Li, Z. Zhang, J. Fu, C. Zhao and E. Xie, *ACS Nano*, 2012, **7**, 174.
[9] L.-F. Cui, L. Hu, J. W. Choi and Y. Cui, *ACS Nano*, 2010, **4**, 3671.
[10] K. H. Seng, J. Liu, Z. P. Guo, Z. X. Chen, D. Jia and H. K. Liu, *Electrochem. Commun.*, 2011, **13**, 383.
[11] J. Ji, L. L. Zhang, H. Ji, Y. Li, X. Zhao, X. Bai, X. Fan, F. Zhang and R. S. Ruoff, *ACS Nano*,

2013, **7**, 6237.

[12] T. Hu, X. Sun, H. Sun, M. Yu, F. Lu, C. Liu and J. Lian, *Carbon*, 2013, **51**, 322.

[13] R. Wang, C. Xu, J. Sun, L. Gao and C. Lin, *J. Mater. Chem. A*, 2013, **1**, 1794.

[14] K. C. Klavetter, J. L. Snider, J. P. de Souza, H. Tu, T. H. Cell, J. H. Cho, C. J. Ellison, A. Heller and C. B. Mullins, *J. Mater. Chem. A*, 2014, **2**, 14459.

Table S2. Superior cycle stability ever reported for manganese oxide-based electrodes for comparison with our results.

Manganese oxide-based electrodes	Electrolyte	C_a (mF/cm^2)	Cycle stability	Ref.
Graphene/MnO_2/ Conducting polymer	0.5 M Na_2SO_4	N/A	95% retention after 3000 cycles	1
Graphene/MnO_2 //Activated carbon nanofibers	1 M Na_2SO_4	N/A	97.3% retention after 1000 cycles	2
GO/MnO_2	1 M Na_2SO_4	N/A	84.1% retention after 1000 cycles	3
Zn_2SnO_4/MnO_2 Nanocable-Carbon Microfiber	1 M Na_2SO_4	N/A	98.8% retention after 1000 cycles	4
WO_{3-x}@Au@MnO_2	0.1 M Na_2SO_4	N/A	110% retention after 5000 cycles	5
Carbon nanoparticles /MnO_2 nanorods	0.1 M Na_2SO_4	109	97.3% retention after 10,000 cycles	6
Three-Dimensional Graphene/MnO_2	0.5 M Na_2SO_4	N/A	81.2% retention after 5000 cycles	7
Two-Dimensional MnO_2/Graphene	PVA/H_3PO_4 gel	N/A	92% retention after 7000 cycles	8
MnO_2 nanowires // Fe_2O_3 nanotubes	PVA/LiCl gel	150	84% retention after 5000 cycles	9
Bacterial-Cellulose-Derived Carbon Nanofiber @ MnO_2 //N-Doped Carbon Nanofiber	1 M Na_2SO_4	N/A	95.4% retention after 2000 cycles	10
MnO_2 Nanowire /Graphene // Graphene	1 M Na_2SO_4	N/A	79% retention after 1000 cycles	11
H-TiO_2 @MnO_2 core-shell NWs //H-TiO_2 @C core-shell NWs	PVA/LiCl gel	N/A	91.2% retention after 5000 cycles	12
Hierarchical $M(OH)_2$/MnO_2 Nanofibril/Nanowires	1 M $LiClO_4$	181	85.2% retention after 1000 cycles	13
Highly Ordered MnO_2 Nanopillars	1 M Na_2SO_4	N/A	93% retention after 5000 cycles	14
Graphen/MnO_2-Textile// CNT-Textile	0.5 M Na_2SO_4	N/A	~95% retention after 5000 cycles	15
Au-doped MnO_2 films	2 M Li_2SO_4	N/A	107% retention after 15,000 cycles	16

Graphene/MnO_2 Nanospheres// Graphene/MoO_3 Nanosheets	1 M Na_2SO_4	N/A	>100% retention after 1000 cycles	17
Nanoporous gold/MnO_2	2 M Li_2SO_4	N/A	~85% retention after 1000 cycles	18
Activated carbon//MnO_2	0.1M K_2SO_4	N/A	~87.5% retention after 195,000 cycles	19
MnO_2	0.1 M Na_2SO_4	N/A	100% retention after 1000 cycles	20
Nickel-manganese oxide	1 M Na_2SO_4	N/A	~88% retention after 10,000 cycles	21
Cobalt-manganese oxide	1 M Na_2SO_4	N/A	~86% retention after 10,000 cycles	21
MnO_2-CNT-sponge	1 M Na_2SO_4	N/A	~96% retention after 100,000 cycles	22
MnO_2/carbon cloth	PVA/H_3PO_4 gel	2.3	>90% retention after 60,000 cycles	23
Manganese Oxide/Graphene Aerogel	0.5 M Na_2SO_4	N/A	95% retention after 100,000 cycles	24
Carbon/MnO_2	5 M $LiNO_3$	N/A	95% retention after 15,000 cycles	25
AC//$NaMnO_2$	0.5 M Na_2SO_4	N/A	97% retention after 10,000 cycles >80% retention after 100,000 cycles	26
Carbon/$LiMn_2O_4$	1 M Li_2SO_4	N/A	95% retention after 20,000 cycles	27
MNGHNs/AGO	1 M Na_2SO_4	173.2	96.1% retention after 5000 cycles 90.2% retention after 200,000 cycles	This work
MNGHNs/AGO	PVA/H_3PO_4 gel	161.0	99.7% retention after 5000 cycles 91.5% retention after 200,000 cycles	This work

References

[1] G. Yu, L. Hu, N. Liu, H. Wang, M. Vosgueritchian, Y. Yang, Y. Cui, Z. Bao, *Nano Lett.* **2011**, 11, 4438.

[2] Z. Fan, J. Yan, T. Wei, L. Zhi, G. Ning, T. Li, F. Wei, *Adv. Funct. Mater.* **2011**, 21, 2366.

[3] S. Chen, J. Zhu, X. Wu, Q. Han, X. Wang, *ACS Nano* **2010**, 4, 2822.

[4] L. Bao, J. Zang, X. Li, *Nano Lett.* **2011**, 11, 1215.

[5] X. Lu, T. Zhai, X. Zhang, Y. Shen, L. Yuan, B. Hu, L. Gong, J. Chen, Y. Gao, J. Zhou, *Adv.*

Mater. **2012**, 24, 938.

[6] L. Yuan, X. H. Lu, X. Xiao, T. Zhai, J. Dai, F. Zhang, B. Hu, X. Wang, L. Gong, J. Chen, *ACS Nano* **2011**, 6, 656.

[7] Y. He, W. Chen, X. Li, Z. Zhang, J. Fu, C. Zhao, E. Xie, *ACS Nano* **2012**, 7, 174.

[8] L. Peng, X. Peng, B. Liu, C. Wu, Y. Xie, G. Yu, *Nano Lett.* **2013**, 13, 2151.

[9] P. Yang, Y. Ding, Z. Lin, Z. Chen, Y. Li, P. Qiang, M. Ebrahimi, W. Mai, C. P. Wong, Z. L. Wang, *Nano Lett.* **2014**, 14, 731.

[10] L. F. Chen, Z. H. Huang, H. W. Liang, Q. F. Guan, S. H. Yu, *Adv. Mater.* **2013**, 25, 4746.

[11] Z. S. Wu, W. Ren, D. W. Wang, F. Li, B. Liu, H. M. Cheng, *ACS Nano* **2010**, 4, 5835.

[12] X. Lu, M. Yu, G. Wang, T. Zhai, S. Xie, Y. Ling, Y. Tong, Y. Li, *Adv. Mater.* **2013**, 25, 267.

[13] J. Duay, S. A. Sherrill, Z. Gui, E. Gillette, S. B. Lee, *ACS Nano* **2013**, 7, 1200.

[14] Z. Yu, B. Duong, D. Abbitt, J. Thomas, *Adv. Mater.* **2013**, 25, 3302.

[15] G. Yu, L. Hu, M. Vosgueritchian, H. Wang, X. Xie, J. R. McDonough, X. Cui, Y. Cui, Z. Bao, *Nano Lett.* **2011**, 11, 2905.

[16] J. Kang, A. Hirata, L. Kang, X. Zhang, Y. Hou, L. Chen, C. Li, T. Fujita, K. Akagi, M. Chen, *Angewandte Chemie* **2013**, 125, 1708.

[17] J. Chang, M. Jin, F. Yao, T. H. Kim, V. T. Le, H. Yue, F. Gunes, B. Li, A. Ghosh, S. Xie, *Adv. Funct. Mater.* **2013**, 23, 5074.

[18] X. Lang, A. Hirata, T. Fujita, M. Chen, *Nat. Nanotechnol.* **2011**, 6, 232.

[19] T. Brousse, P. L. Taberna, O. Crosnier, R. Dugas, P. Guillemet, Y. Scudeller, Y. Zhou, F. Favier, D. Bélanger and P. Simon, *J. Power Sources*, 2007, **173**, 633.

[20] M. Toupin, T. Brousse and D. Bélanger, *Chem. Mater.*, 2002, **14**, 3946.

[21] H. Kim and B. N. Popov, *J. Electrochem. Soc.*, 2003, **150**, D56.

[22] W. Chen, R. Rakhi, L. Hu, X. Xie, Y. Cui and H. Alshareef, *Nano Lett.*, 2011, **11**, 5165.

[23] L. Wu, R. Li, J. Guo, C. Zhou, W. Zhang, C. Wang, Y. Huang, Y. Li and J. Liu, *AIP Advances*, 2013, **3**, 082129.

[24] C. C. Wang, H. C. Chen and S. Y. Lu, *Chem.-Eur. J.*, 2014, **20**, 517.

[25] H. Mosqueda, O. Crosnier, L. Athouël, Y. Dandeville, Y. Scudeller, P. Guillemet, D. Schleich and T. Brousse, *Electrochim. Acta*, 2010, **55**, 7479.

[26] Q. Qu, Y. Shi, S. Tian, Y. Chen, Y. Wu and R. Holze, *J. Power Sources*, 2009, **194**, 1222.

[27] Y. G. Wang and Y. Y. Xia, *Electrochem. Commun.*, 2005, **7**, 1138.

Table S3. Performance comparison of both carbon-based materials and non-carbon-based materials (including metal oxides, sulfides, nitrides etc.) for two-electrode supercapacitors (including symmetric SCs (SSCs) and asymmetric SCs (ASCs)), along with typical literature results for commercial supercapacitors, based on whole volume of the SCs stack—including two electrodes, electrolyte, a separator between two electrodes, and current collectors.

Electrode Materials		Electrolyte	C_v (F/cm^3)	Energy Density (mWh/cm^3)	Ref.
Carbon-based materials	Laser Scribing Graphene-SSCs	PVA/H_3PO_4 gel	~0.43	~0.06	1
	Laser Scribing Graphene-SSCs	$TEA\text{-}BF_4/CH_3CN$	0.59	~0.74	1
	Laser Scribing Graphene-SSCs	Ionic liquid	0.61	1.36	1
	PANASONIC 2.75 V/44mF Commercial AC-EC	N/A	~0.68	~0.72	1
	Graphene Hydrogel-SSCs	PVA/H_2SO_4 gel	31	1.92	2
	Commercial Activated Carbon-SSCs	Aqueous electrolyte	80~110	5~8	3
	Commercial Activated Carbon-SSCs	Organic electrolyte	60~120	N/A	3
	Activated carbon-SSCs	PEO/KOH	~3.7	0.33~0.44	4
	Hydrated Graphite Oxide-SSCs	H_2O	3.1	0.43	5
	Onion-Like Carbon-SSCs	Et_4NBF_4/PC	1.3	~1.5	6
	Activated Carbon-SSCs	Et_4NBF_4/PC	9.0	10	6
Non-carbon-based materials	VN/CNT-SSCs	PVA/H_3PO_4 gel	7.9	0.54	7
	VOx//VN-ASCs	PVA/LiCl gel	1.35	0.61	8
	TiN on carbon fabric-SSCs	PVA/KOH gel	0.33	0.05	9
	Carbon/MnO_2-SSCs	PVA/H_3PO_4 gel	2.5	0.12	10
	ZnO@amorphous ZnO-doped MnO_2-SSCs	PVA/LiCl gel	0.325	0.04	11
	TiO2@carbon fabrics-SSCs	PVA/H_2SO_4 gel	0.125	0.011	12
	H-TiO_2@MnO_2//H-TiO_2@C-ASCs	PVA/LiCl gel	0.71	0.3	13
	Co_9S_8//Co_3O_4@RuO_2-ASCs	PVA/KOH gel	4.82	1.21	14

	ZnO@MnO_2//RGO-ASCs	PVA/LiCl gel	0.52	0.234	15
Ourmaterials	MNGHNs/AGO-SSCs	PVA/H_3PO_4 gel	26.3	2.34	This work

References

[1] M. F. El-Kady, V. Strong, S. Dubin, R. B. Kaner, *Science* **2012**, 335, 1326.

[2] Y. Xu, Z. Lin, X. Huang, Y. Liu, Y. Huang, X. Duan, *ACS Nano* **2013**, 7, 4042.

[3] X. Yang, C. Cheng, Y. Wang, L. Qiu, D. Li, *Science* **2013**, 341, 534.

[4] A. Lewandowski, M. Zajder, E. Frąckowiak, F. Beguin, *Electrochim. Acta* **2001**, 46, 2777.

[5] W. Gao, N. Singh, L. Song, Z. Liu, A. L. M. Reddy, L. Ci, R. Vajtai, Q. Zhang, B. Wei, P. M. Ajayan, *Nat. Nanotechnol.* **2011**, 6, 496.

[6] D. Pech, M. Brunet, H. Durou, P. Huang, V. Mochalin, Y. Gogotsi, P. L. Taberna, P. Simon, *Nat. Nanotechnol.* **2010**, 5, 651.

[7] X. Xiao, X. Peng, H. Jin, T. Li, C. Zhang, B. Gao, B. Hu, K. Huo, J. Zhou, *Adv. Mater.* **2013**, 25, 5091.

[8] X. Lu, M. Yu, T. Zhai, G. Wang, S. Xie, T. Liu, C. Liang, Y. Tong, Y. Li, *Nano Lett.* **2013**, 13, 2628.

[9] X. Lu, G. Wang, T. Zhai, M. Yu, S. Xie, Y. Ling, C. Liang, Y. Tong, Y. Li, *Nano Lett.* **2012**, 12, 5376.

[10] X. Xiao, T. Li, P. Yang, Y. Gao, H. Jin, W. Ni, W. Zhan, X. Zhang, Y. Cao, J. Zhong, *ACS Nano* **2012**, 6, 9200.

[11] P. Yang, X. Xiao, Y. Li, Y. Ding, P. Qiang, X. Tan, W. Mai, Z. Lin, W. Wu, T. Li, *ACS Nano* **2013**, 7, 2617.

[12] H. Zheng, T. Zhai, M. Yu, S. Xie, C. Liang, W. Zhao, S. C. I. Wang, Z. Zhang, X. Lu, *J. Mater. Chem. C* **2013**, 1, 225.

[13] X. Lu, M. Yu, G. Wang, T. Zhai, S. Xie, Y. Ling, Y. Tong, Y. Li, *Adv. Mater.* **2013**, 25, 267.

[14] J. Xu, Q. Wang, X. Wang, Q. Xiang, B. Liang, D. Chen, G. Shen, *ACS Nano* **2013**, 7, 5453.

[15] Z. Wang, Z. Zhu, J. Qiu, S. Yang, *J. Mater. Chem. C* **2014**, 2, 1331.